Supplementary Material to "Evolution of Saturn's Mid-Sized Moons"

Marc Neveu, Alyssa R. Rhoden

February 6, 2019

We have developed an enhanced implementation of the thermal-orbital code in which moon-moon interactions are computed with an averaged Hamiltonian model, in order to assess the accuracy of the rougher model of moon-moon interactions treated as encounters described in the main text. Here, we describe the implementation and validation of the averaged Hamiltonian model (Supplementary §1). We describe results obtained with this improved model (Supp. §2), and show that their behavior matches that obtained with the more simplistic treatment of moon-moon interactions described in the Methods (Supp. §3). Given limitations described below of the averaged Hamiltonian model in high-eccentricity cases, which affect resonance capture and escape and runaway internal heating by tidal dissipation (two essential aspects of the moons' evolution), we choose to use the simplified model. In spite of the limitations of either model, similarities in outcomes suggest that general features of the moons' orbital evolution are robustly captured.

1 Averaged Hamiltonian orbital model

In this implementation, the code calls N parallel instances (here, $N = 5$) of the thermal subroutine and an additional orbital evolution subroutine. Both subroutines are run for one time step; the orbital subroutine returns the updated orbital parameters (a and e) of its corresponding moon to the main program, which feeds orbital parameters for all moons into each orbital evolution subroutine instance at the next time step.

We implement the model described in Appendix A of Meyer and Wisdom (2008) (noting typos in their equation (A.23) – m_i instead of m_0 – and in their equation (A.30), where the inverse of the denominator need not be taken) using a 10-substep modified midpoint method (Press et al., 2002). This model is only valid for $j + k : j$ orbit-orbit resonances with $k = 1$, but could be expanded to accommodate higher k with additional coefficients (Murray and Dermott, 1999). In this model, resonant orbital evolution is computed only between pairs of moons, using an averaged Hamiltonian approximation rather than a full N-body approach. This prevents us from accurately computing the orbital evolution of a moon in mean-motion resonance with more than one other moon, but enables much faster semi-analytical computations of a and e.

We benchmarked our implementation against previous results on the orbital evolution of Enceladus and Dione through the 2:1 resonance (Meyer and Wisdom, 2008; Zhang and Nimmo, 2009). Benchmark results are shown in Supplementary Fig. 6. The values we adopt to compute the effect of Saturn's oblateness (zonal gravity harmonics $J_2 = 16290.71 \times 10^{-6}$, $J_4 = -935.83 \times 10^{-6}$; Jacobson et al. (2006)) on the precession of orbits and resonant angles yield orbital precession rates for Enceladus (161 deg yr^{-1}) and Dione (32 deg yr^{-1}), calculated using equations (A.11) and (A.12) of Meyer and Wisdom (2008), that are higher than those reported by Zhang and Nimmo (2009): 88.4 deg yr^{-1} and 17.5 deg yr^{-1}, respectively. We could not find an obvious explanation for this discrepancy. Higher precession rates only act to further spread apart in time the components of any orbit-orbit resonance.

Our simulations of the Enceladus-Dione 2:1 resonance produce values for orbital parameters in quantitative agreement with those previously computed (Meyer and Wisdom, 2008; Zhang and Nimmo, 2009) within each of the steps through the 2:1 resonance (Supplementary Fig. 6). These benchmark simulations yield identical results with time steps of 5×10^{-4} and 5×10^{-5} years, but such numerical convergence is not achieved with a time step of 5×10^{-3} years. Therefore, we adopt a time step of 5×10^{-4} years ≈ 0.2 days, just a few time steps per orbit.

Because this averaged Hamiltonian model implements tidal equations (4) (without the ring torque term) and (5) described in the Methods (Meyer and Wisdom, 2008), our code switches between using solely these equations during secular evolution of a given moon (even if other moons in the system are in resonance) and the averaged Hamiltonian model during resonant evolution. This piecewise approach was adopted previously (Zhang and Nimmo, 2009) to keep computation times reasonable. The averaged Hamiltonian routine is called only for pairs of moons whose mean motion ratio comes within 1% of a commensurability, and as long as it remains within 1.5% of it. The latter threshold is higher to avoid moons spuriously going in and out of resonance if the mean motion ratio crosses the capture condition back and forth immediately after capture. The choice of commensurability threshold is arbitrary because the width of a resonance is not well known (Malhotra, 1998). We consider orbit-orbit resonances up to $j = 5$, i.e. from 2:1 to 6:5.

Tidal evolution is sped up by a factor 10^3, such that the main code, within a 50-year time step, calls the resonant orbital evolution routine $50/(5 \times 10^{-4})/10^3 = 100$ times. Using such speed-up factors has been shown not to affect the computation of resonant orbital evolution, as long as they remain lower than the ratio between the time scales of secular tidal evolution and resonant angle libration (e.g. Meyer and Wisdom, 2008; Zhang and Nimmo, 2009).

We ignore resonant interactions if the moons are still gravitationally interacting with the rings, assuming that fast orbital expansion resulting from the ring torque prevents capture into resonance. Finally, we arbitrarily set eccentricities below 10^{-7} to 10^{-7} so that $e^2 > 1.1 \times 10^{-16}$, the machine double precision, to avoid singularities in the implementation of the model, which involves a division by $1 - \sqrt{1 - e^2}$ to compute the angular momentum associated with a moon's osculating orbit (Meyer and Wisdom, 2008, equation A.7).

The equations of this model were derived under the assumption of small eccentricities

(Meyer and Wisdom, 2008), and become increasingly inaccurate for increasing eccentricities. Because excitation to high eccentricities can induce significant changes in semi-major axes Δa owing to angular momentum conservation given that $\Delta a/a \sim j\Delta e^2$ (Malhotra, 1998, their equation 26), these changes are also not accurately computed.

2 Simulations with averaged Hamiltonian model

Results of simulations with the model of Supp. §1 are shown in Supp. Fig. 7–11. The cases shown in Supp. Fig. 7, 8, and 9 are similar to those simulated with the more simplistic model of moon-moon interactions shown in Fig. 2 (initial Saturn $Q = 80000$). Those shown in Supp. Fig. 10 and 11 are similar to those shown in Fig. 3 (constant $Q \approx 2450$) and Supp. Fig. 3 (initial $Q = 20000$), respectively. Starting conditions for all simulations are shown in Table 1.

Supp. Fig. 7: As in Fig. 2, Saturn's Q is set to 80000 initially, linearly decreasing to near 2450 at the present day. In the first Gyr, Dione's eccentricity is excited by passage through the 3:2 resonance with Tethys to values above 0.1 that allow sufficient solid tidal dissipation to melt ice in its shell and emplace a short-lived ocean. The resonance is escaped after 14 Myr once Dione's e is high enough.

The computed exchange of angular momentum with Tethys shrinks Dione's orbit, bringing it fast toward 2:1 resonance with Enceladus. Because Dione's eccentricity has not decayed enough when it encounters this resonance, there is no capture. Instead, Enceladus' semi-major axis experiences a brief but large increase due to transfer of angular momentum from Dione's eccentric orbit (Malhotra, 1998; Meyer and Wisdom, 2008, their equations A.5-A.7). Although this increase, computed outside the small-e regime, may be inaccurate (Supp. §1), Enceladus' resulting semi-major axis becomes too high to be compatible with its present-day position.

If indeed the 2:1 Enceladus-Dione resonance moves Enceladus past its current orbit if Dione's eccentricity is high, i.e. if Dione's 2:1 resonance with Enceladus happens just after its 3:2 resonance with Tethys, the observed orbital configuration requires that these resonances are further apart in time so Dione's e has time to decay and capture can occur.

This happens if Dione starts further out, because the secular expansion of Tethys' orbit is faster than Enceladus', such that Tethys encounters the 3:2 resonance with Dione when Enceladus is still far inward of the 2:1 resonance with Dione. This case is simulated in Supp. Fig. 8. Another scenario compatible with a starting Saturn Q of 80000 is that Enceladus forms a few 0.1 Gyr after Dione escapes the 3:2 resonance with Tethys. This is the case explored in Supplementary Fig. 9.

Supp. Fig. 8: Indeed, starting Dione further out allows its eccentricity to decay enough after 3:2 resonance with Tethys to allow capture in the 2:1 resonance with Enceladus. However, within 20 Myr Dione's e is excited to 0.09 and it escapes this resonance.

Angular momentum is imparted in Enceladus' orbit, here too expanding it beyond the observed semi-major axis. Its eccentricity increases only to a few 10^{-2}. The orbit subsequently does not circularize, as Enceladus' frigid interior is not dissipative: radiogenic

Parameter	Mimas	Enceladus	Tethys	Dione	Rhea
Supp. Fig. 1: initial Q: 80000, final ring mass: 5×10^{19} kg					
Time of formation (Myr)	4290	primordial	primordial	primordial	primordial
Initial semi-major axis (km)	160000	160000	270000	363000	523000
Supp. Fig. 2: initial Q: 50000, final ring mass: 1×10^{19} kg					
Time of formation (Myr)	3450	3200	primordial	primordial	primordial
Initial semi-major axis (km)	160000	160000	160000	356000	521000
Supp. Fig. 3: initial Q: 20000, final ring mass: 1×10^{19} kg					
Time of formation (Myr)	3450	3400	3200	primordial	primordial
Initial semi-major axis (km)	160000	160000	160000	330000	515000
Supp. Fig. 7: initial Q: 80000, final ring mass: 1.5×10^{19} kg					
Time of formation (Myr)	4117	primordial	primordial	primordial	primordial
Initial semi-major axis (km)	160000	160000	270000	358000	523000
Supp. Fig. 8: initial Q: 80000, final ring mass: 1.5×10^{19} kg					
Time of formation (Myr)	4117	primordial	primordial	primordial	primordial
Initial semi-major axis (km)	160000	160000	270000	363000	523000
Supp. Fig. 9: initial Q: 80000, final ring mass: 1.5×10^{19} kg					
Time of formation (Myr)	4117	600	primordial	primordial	primordial
Initial semi-major axis (km)	160000	160000	270000	357000	523000
Supp. Fig. 10: initial Q: 2452.8, final ring mass: 1.5×10^{19} kg					
Time of formation (Myr)	3830	3600	3500	2200	primordial
Initial semi-major axis (km)	160000	160000	160000	160000	478000
Supp. Fig. 11: initial Q: 20000, final ring mass: 1.5×10^{19} kg					
Time of formation (Myr)	4235	3540	1500	primordial	primordial
Initial semi-major axis (km)	160000	160000	160000	300000	502000

Table 1: **Initial conditions for the simulations shown in this Supplementary Material.** For simulations shown in Supplementary Fig. 1 through 5, the repeated encounter model of moon-moon interactions is used. For those shown in Supplementary Fig. 7 and following, the averaged Hamiltonian model is used. All other parameters are as in Table 1 of the main article.

heating has long since faded and heating from eccentricity tides is insufficient at $e \sim 0.01$. Thus, Enceladus' orbital and internal characteristics do not match those observed today. This simulation ends in orbit crossing spurred by the Tethys-Dione 4:3 resonance.

Supp. Fig. 9: Forming Enceladus after Dione escapes the 3:2 resonance with Tethys also allows Dione's eccentricity to decay before the 2:1 resonance with Enceladus is encountered, such that capture occurs at 1 Gyr. In this case, Enceladus' eccentricity (rather than semi-major axis) is excited more than Dione's, allowing the resonance to persist intermittently over billions of years. The intermittency results from contraction of Enceladus' orbit by transfer of angular momentum into Dione's: whenever it contracts back into the rings' zone of influence ($a \leq 222000$ km), the code forces the resonance to break (§1).

The resonance is finally escaped at 4.4 Gyr, when Dione encounters a 4:3 resonance with Tethys that excites its eccentricity above 0.1, melting part of its ice shell. This, amplified by rapid migration due to Saturn's low Q beyond 4.6 Gyr (the assumed linear decrease leading to non-physical negative values shortly thereafter), sends Dione and Tethys on a collision course that ends the simulation.

Enceladus' eccentricity is never high enough to induce melting. Later in its evolution, its eccentricity increases over time due to its interactions with Dione, without decaying as much. Under slightly different conditions (e.g. plateauing Saturn Q), it could be that its eccentricity ends up high enough to induce melting and re-circularization, but we did not explore such scenarios.

Supp. Fig. 10: As with Fig. 3, Saturn's Q is set to the constant, low present-day value of 2452.8. Consequently, orbital expansion is fast: only Rhea is primordial. Dione forms shortly after 2 Gyr and encounters a 2:1 resonance with Rhea just before 3 Gyr. This strong resonance between the two relatively massive moons leads to the sudden expansion of Dione's orbit, crossing the 3:2 and 4:3 resonances, and excitation of Rhea's eccentricity to 0.3. Around 3.25 Gyr, the moons encounter the 5:4 resonance that leads to the ejection of Rhea, terminating the simulation before the inner moons form.

Supp. Fig. 11: As with Supplementary Fig. 3, Saturn's Q is set to 20000 initially and decreases linearly to the present-day value. The orbits of all moons expand roughly at the rate set by Saturn's $Q(t)$, although intermittent resonances tend to place Enceladus, Tethys, and Dione near the 6:4:3 commensurabilities between 3 and 4.5 Gyr. These lead to eccentricity excitation for each moon that generates a short-lived ocean inside Dione, but not elsewhere. The resonances are intermittent because they are exited either due to eccentricities being too high, or due to Enceladus' orbit contracting back to the zone of interaction with the rings. Eventually, as Saturn's Q decreases to low values beyond the present day, rapid migration leads to a resonant encounter between Tethys and Dione that sends the former inward, which in turn sends Enceladus on to an orbit beyond Rhea's.

Stalling artifacts: The simulation shown in Supp. Fig. 7 stalled and was restarted in three instances at 1.07, 1.40, and 1.75 Gyr. The stalling seems due to handling of input/output calls by the operating system such as printout commands simultaneously called by two parallel threads. Similarly, the Supp. Fig. 8 run stalled at 3.05, 3.55, and 3.84 Gyr; the Supp. Fig. 9 run at 0.96, 1.56, 2.24, 2.63, and 3.02 Gyr; the Supp. Fig. 10

run at 0.28, 1.07, 1.93, 2.80, and 2.92 Gyr; and the Supp. Fig. 11 run at 1.49, 2.21, 2.99, and 3.58 Gyr.

Stalled simulations were restarted from the last time output. However, liquid in the interior of a moon prior to stalling can lead to a slight mismatch in internal temperatures and melting after the restart because of feedbacks between conductive and parameterized convective heat transfer. These artifacts are indicated in bottom panels of the respective figures ("Code restarts"), also slightly affecting tidal dissipation (e.g. Supp. Fig. 7, top panel, third from left, pink curve) and the rate of eccentricity decay (second from left, pink curve). The stalling issue only affected simulations performed with the averaged Hamiltonian subroutine and did not affect outcomes in any major way, as assessed with comparisons (not shown) between simulations with identical inputs that stalled at a different times.

3 Assessment of the canonical simulations based on results obtained with the averaged Hamiltonian model

The averaged Hamiltonian model and the repeated encounter model of moon-moon interactions (Methods) lead to fast eccentricity excitation to comparable maximum values. What the repeated encounter model cannot capture are any changes in semi-major axes due to moon-moon interactions, which can be significant. Furthermore, simulations with the latter model allow eccentricity excitation between moons whose migration is divergent, even though capture should not occur in these cases. These are noted when they occur (Fig. 2 and Supp. Fig. 1–5). Although the eccentricities of the moons involved are spuriously excited, the simulations are not affected in any major way.

A key feature of the simulation shown in Fig. 2 with the repeated encounter model is the 4:3 Tethys-Enceladus resonance that generates Enceladus' ocean. Although Tethys and Enceladus' orbits expand secularly in a divergent way, the expansion is convergent shortly before the onset of the resonance because Tethys' orbit is contracting due to high dissipation in its interior, following passage through the 3:2 resonance with Dione. This allows capture into resonance.

Finally, the simulations with the averaged Hamiltonian model suggest that collisions are not uncommon (Supplementary Fig. 8). This lends credence to the hypothesis of several generations of disrupted and re-accreted moons, as previously postulated (Asphaug and Reufer, 2013; Ćuk et al., 2016; Salmon and Canup, 2017). Possible evidence of such events may be the unique geology of Uranus' moon Miranda. In addition, simulated ejections (Supplementary Fig. 10) suggest the possibility of more moons in the past, a hypothesis that was not explored in this work.

Supplementary Figures

(shown on following pages)

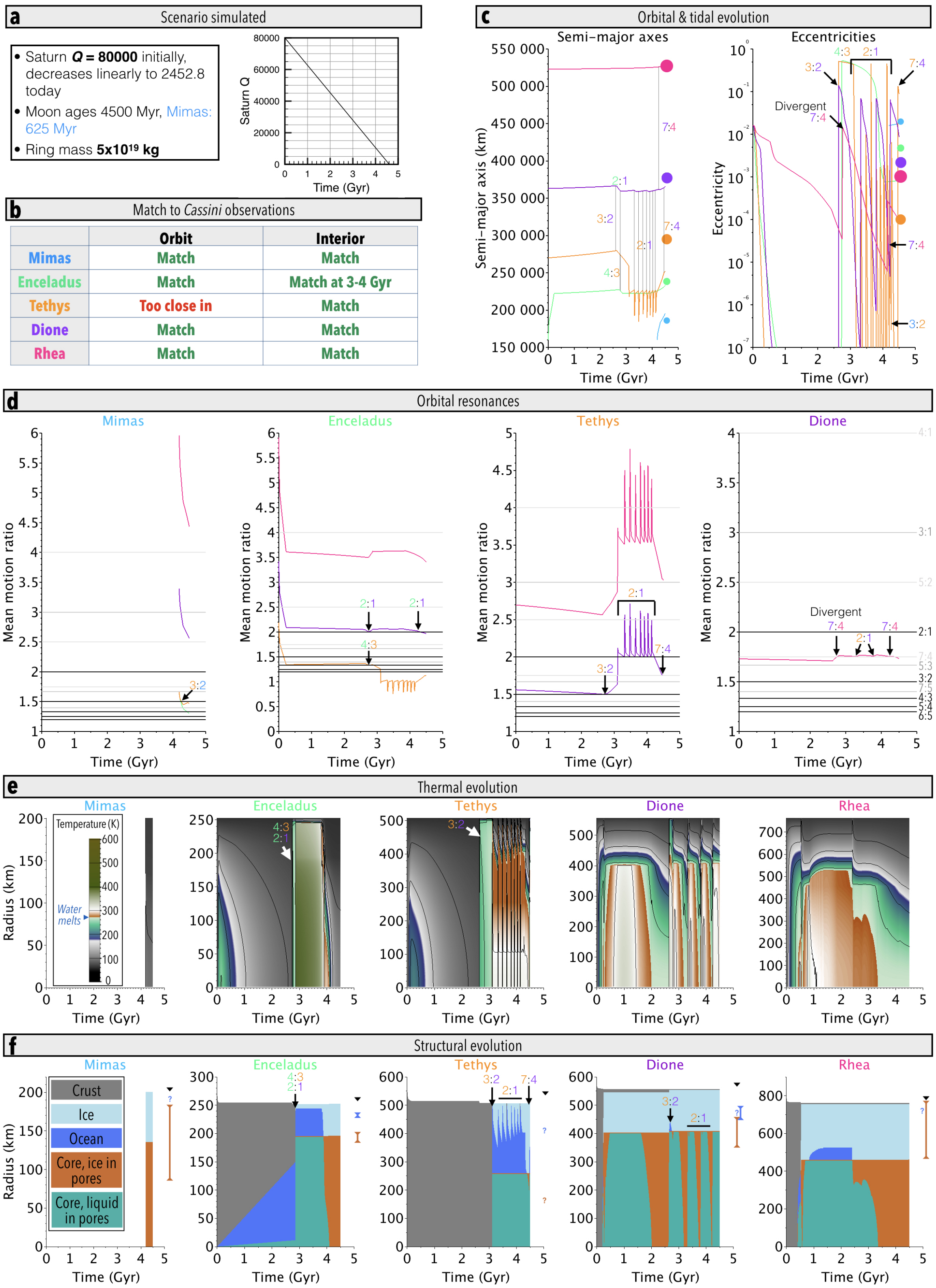

Figure 1: **Orbital, structural, and thermal evolution of Saturn's mid-sized moons for an initial Saturn Q of 80000 and a ring mass of 5×10^{19} kg.** The legend for panel b and panels c-f is the same as for Table 3 and Fig. 2, respectively. Here, Enceladus' ocean refreezes before Mimas forms.

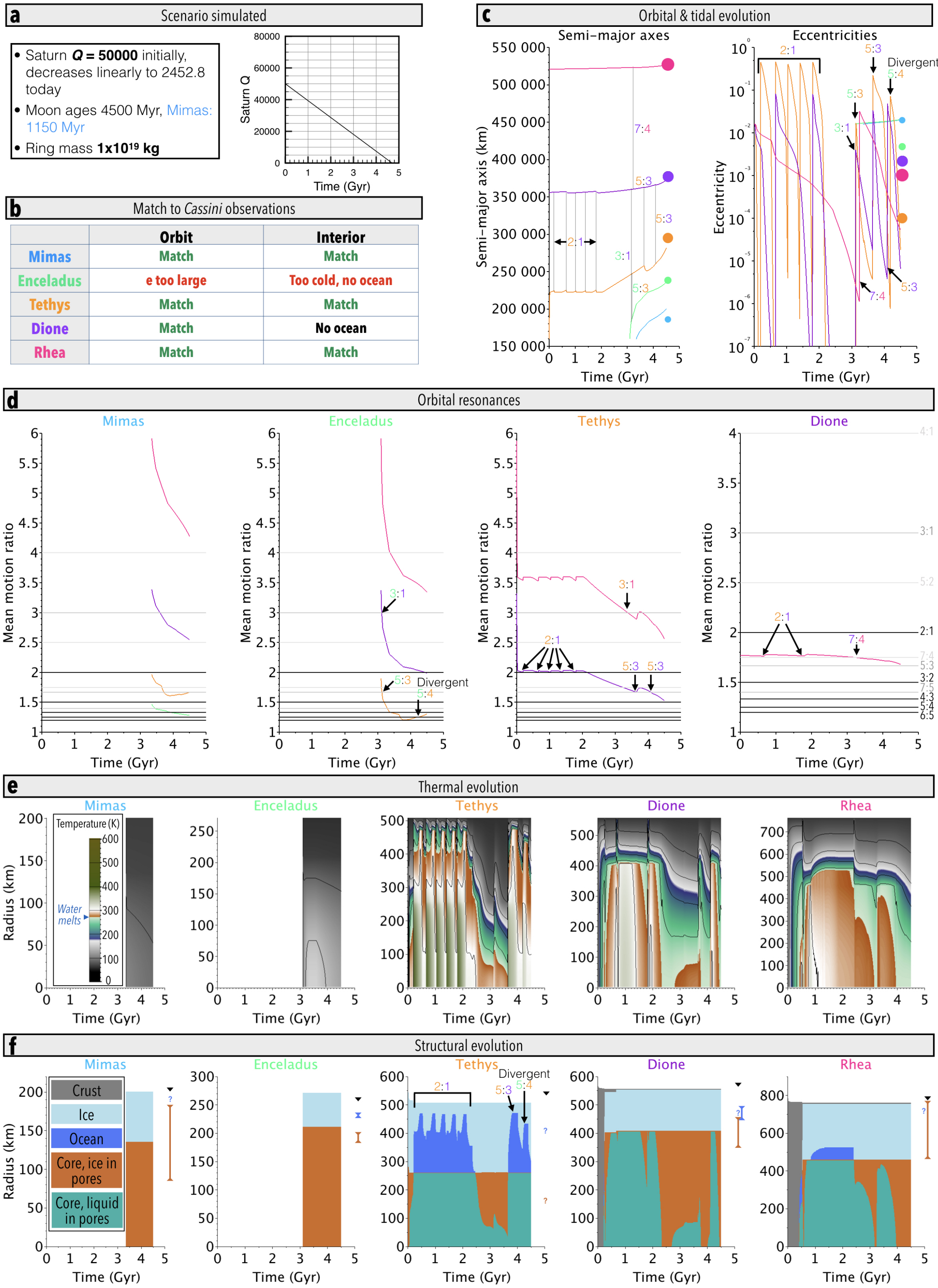

Figure 2: **Orbital, structural, and thermal evolution of Saturn's mid-sized moons for an initial Saturn Q of 50000.** The legend is the same as for Supp. Fig. 1. A ring mass of 1×10^{19} kg is assumed. Compared to Fig. 2, Enceladus forms later and does not differentiate or warm up substantially.

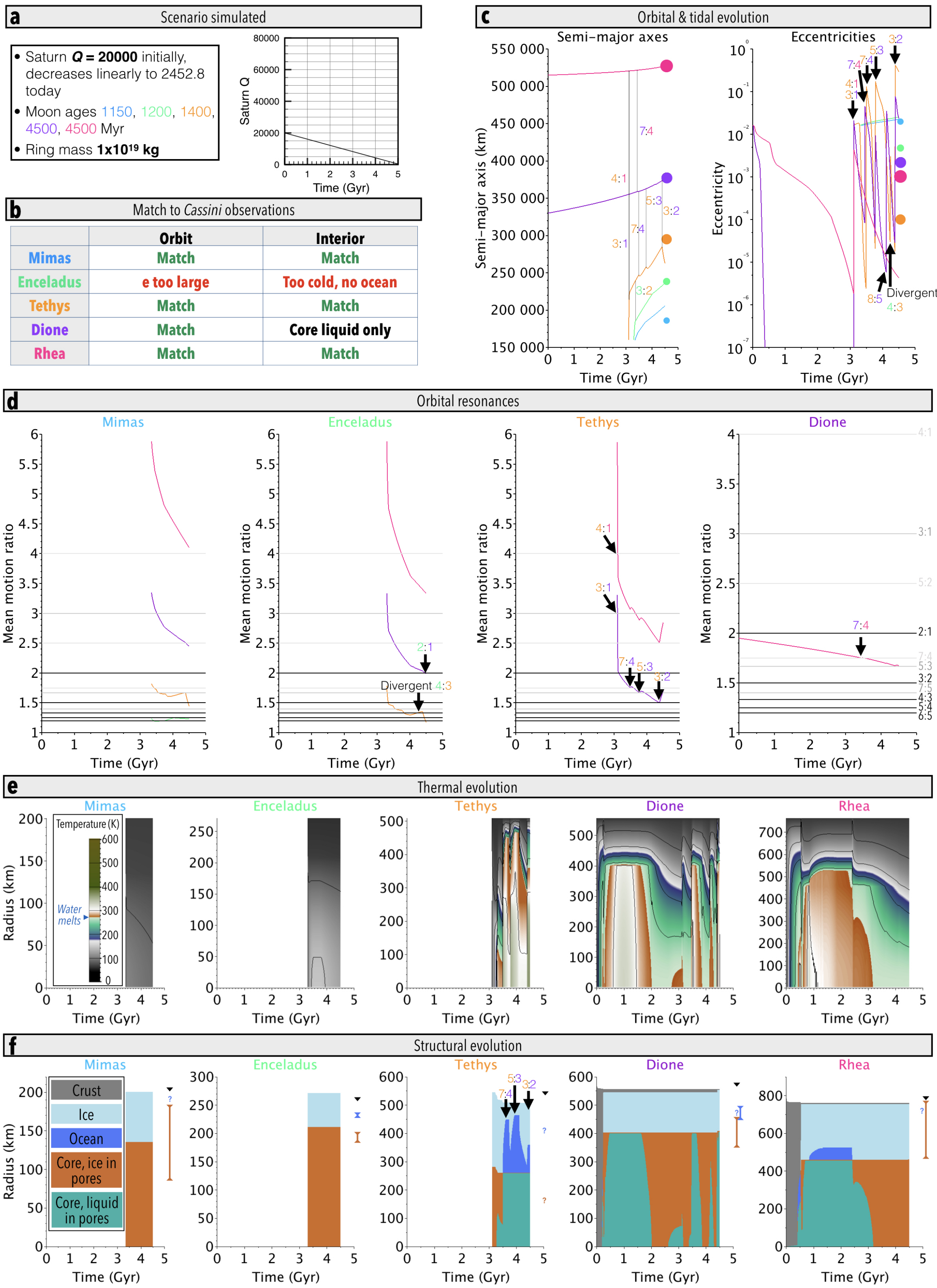

Figure 3: **Orbital, structural, and thermal evolution of Saturn's mid-sized moons for an initial Saturn Q of 20000.** The legend is the same as for Supp. Fig. 1. A ring mass of 1×10^{19} kg is assumed. Compared to Fig. 2, Enceladus does not differentiate or warm up substantially.

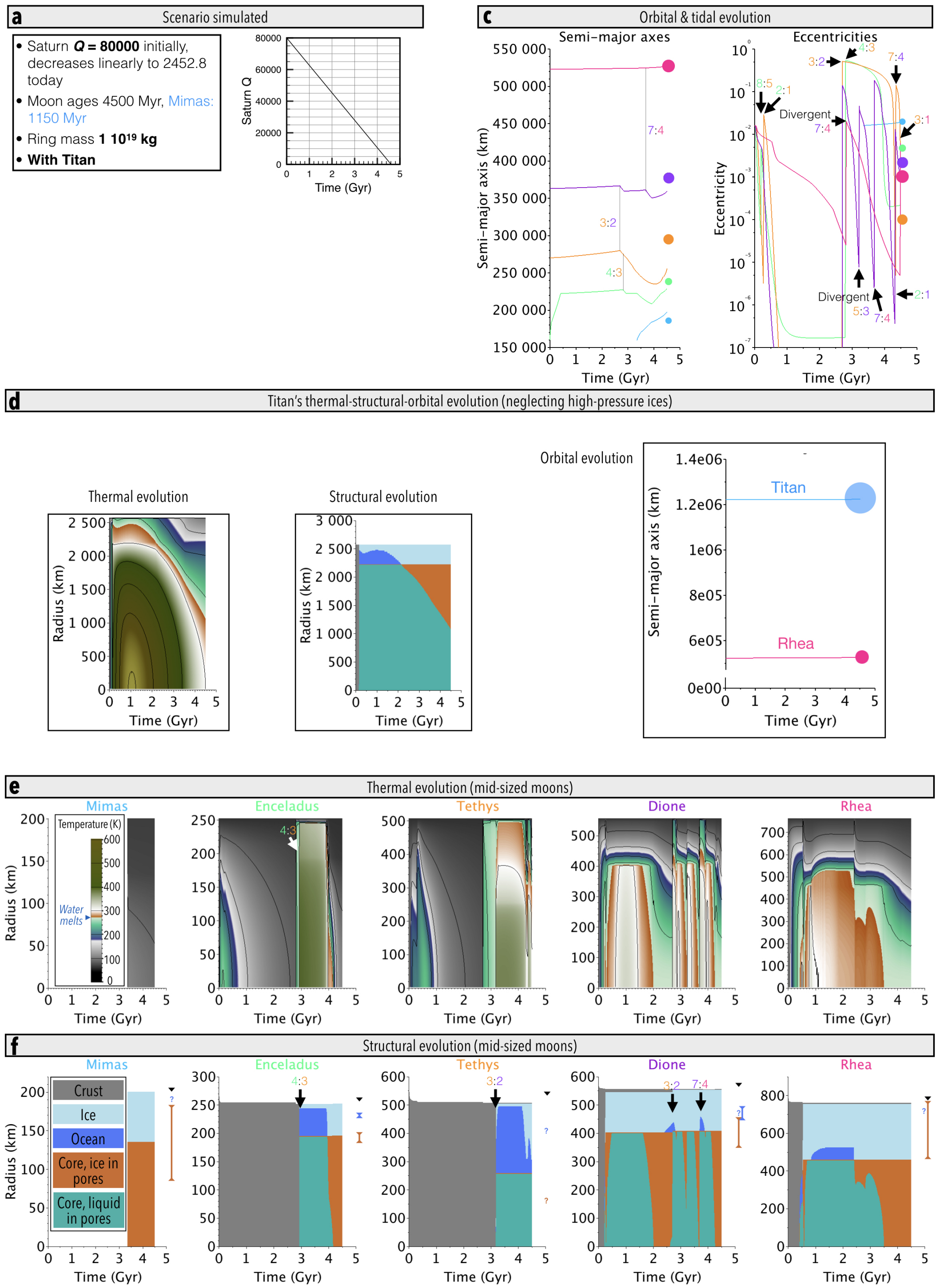

Figure 4: **Orbital, structural, and thermal evolution of Saturn's mid-sized moons for the same case shown in Fig. 2, but with an additional moon with the size and mass of Titan.** This control simulation shows that the results shown in Fig. 2 are not affected by neglecting Titan in the system. In panel (d), the thermal, structural, and orbital evolution of Titan are shown. We compute a spuriously larger core than Titan's (Baland et al., 2014; Sohl et al., 2014) because we neglect both self-compression and high-pressure phases of ice. The legend is otherwise the same as for Supp. Fig. 1.

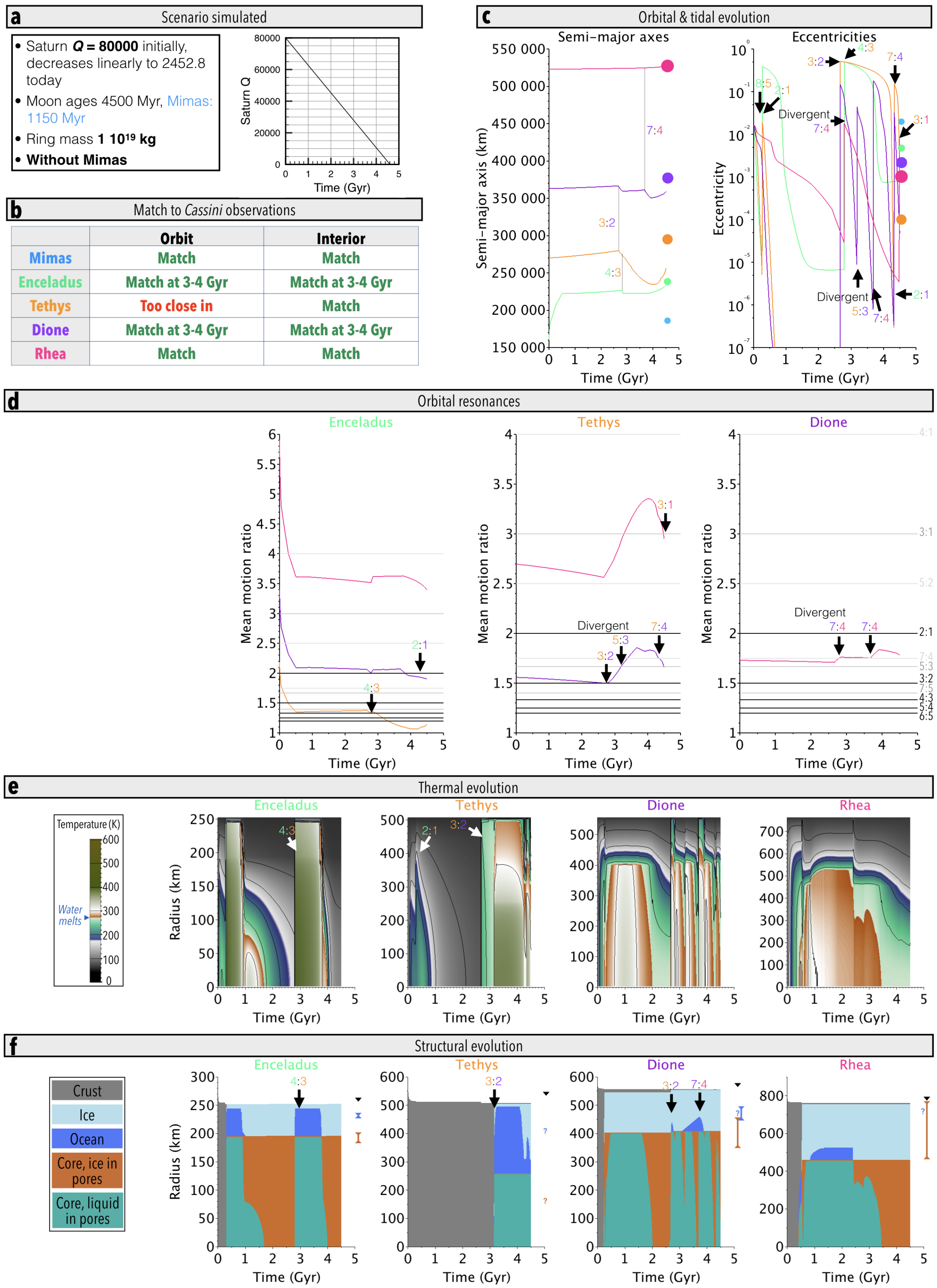

Figure 5: **Orbital, structural, and thermal evolution of Saturn's mid-sized moons for the same case shown in Supplementary Fig. 1, except that Mimas is absent from the simulation.** The legend is the same as for Supp. Fig. 1. This control simulation shows that the main results are not affected by neglecting the growth of a late-forming Mimas over time.

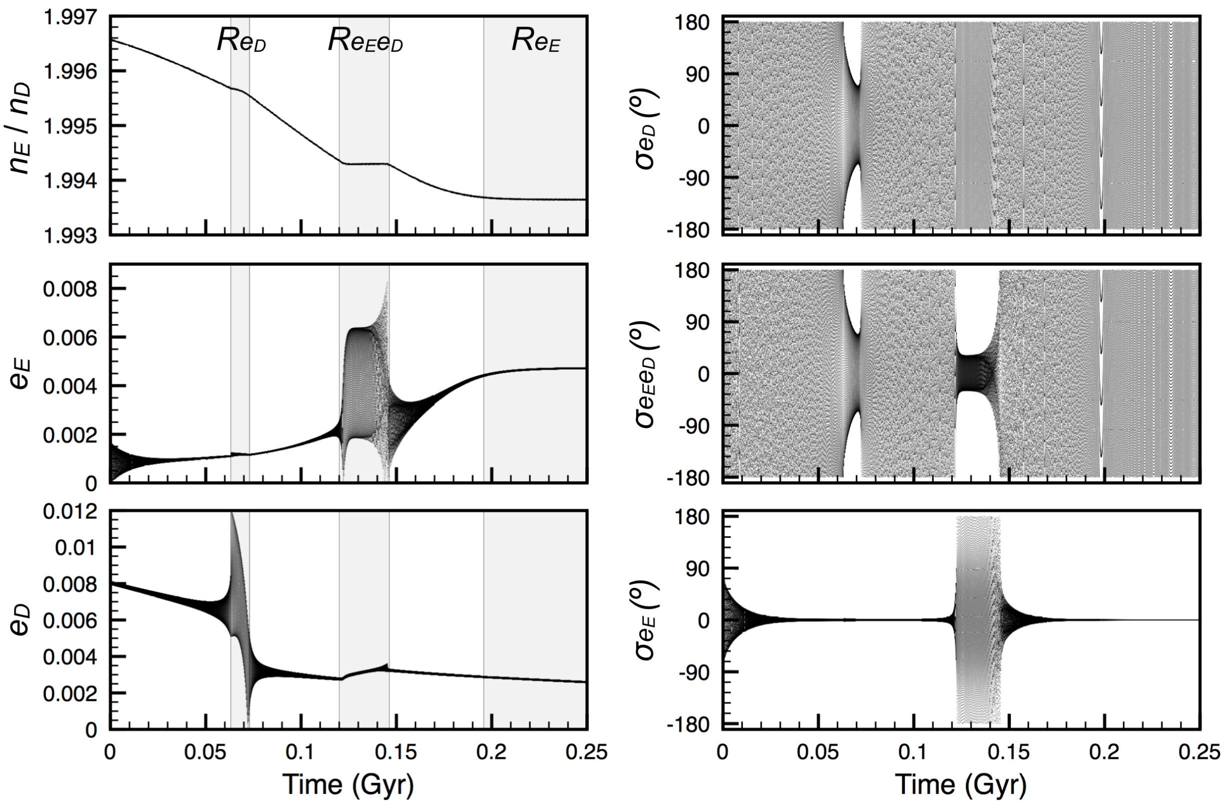

Figure 6: **Benchmark simulation for the averaged Hamiltonian model of moon-moon interactions.** The simulated recent past evolution of Enceladus and Dione through the 2:1 mean-motion resonance is similar to that modeled by Meyer and Wisdom (2008, their Fig. 10 and 11) and with an N-body code (Zhang and Nimmo, 2009, their Fig. 2). Left panels: ratio of the mean motion of Enceladus n_E to that of Dione n_D (top), eccentricity of Enceladus e_E (middle), and eccentricity of Dione e_D (bottom) over time. Right panels: resonant angle for the e-Dione (top), second-order e-Enceladus-e-Dione (middle), and e-Enceladus (bottom) sub-resonances of the overall 2:1 resonance. These are separated in time due to orbital precession induced by Saturn's oblateness. The abscissae display real time, i.e. computed time multiplied by the speed-up factor 10^3.

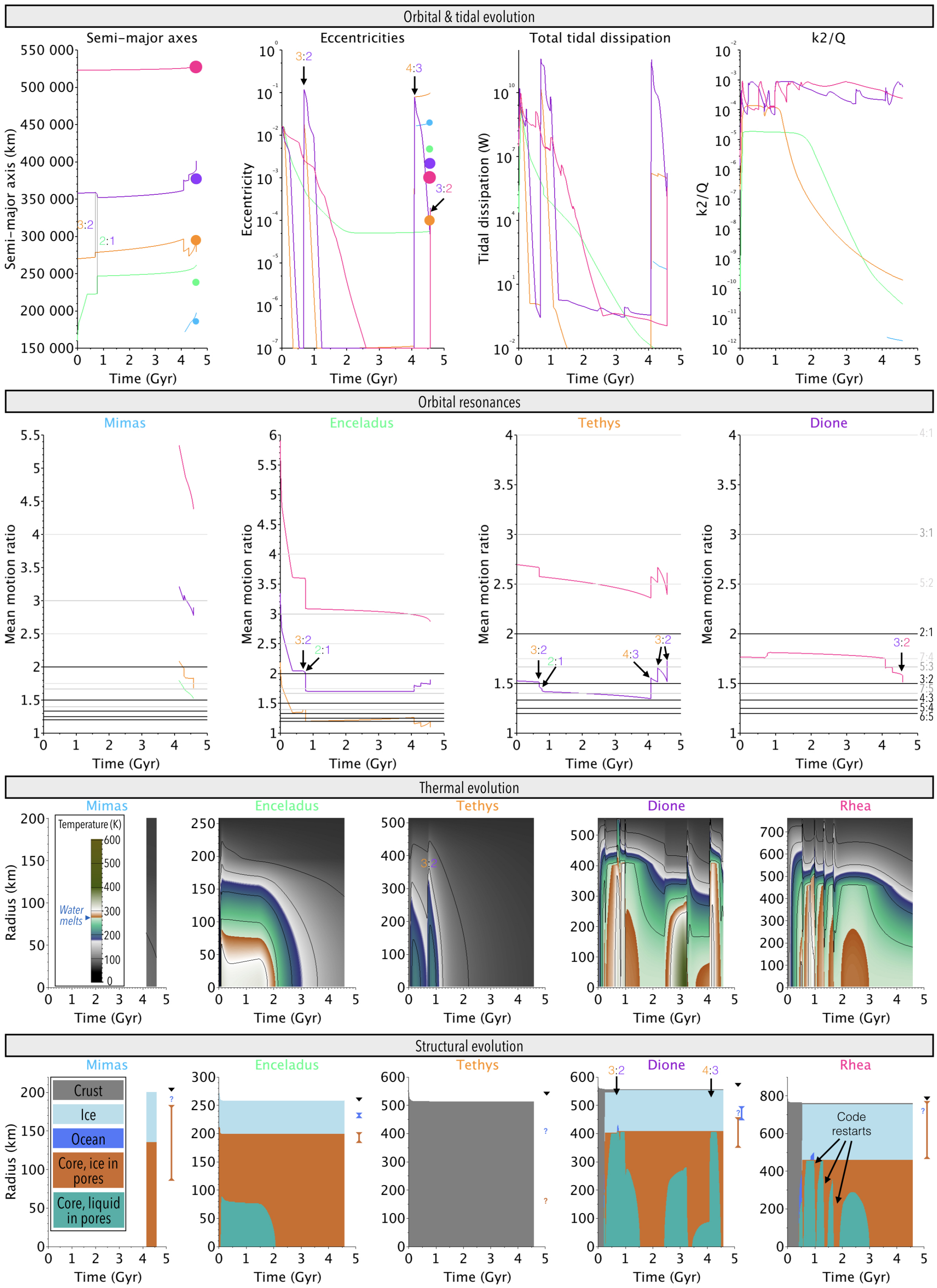

Figure 7: **Orbital, structural, and thermal evolution of Saturn's mid-sized moons for a case similar to that shown in Fig. 2 (Saturn Q=80000 initially), but with the averaged Hamiltonian model.** In the bottom three panels, the same quantities as in Supp. Fig. 1 are shown. In the top panel are displayed, in addition to semi-major axes and eccentricities, computed total dissipation and equivalent k_2/Q of each moon over time.

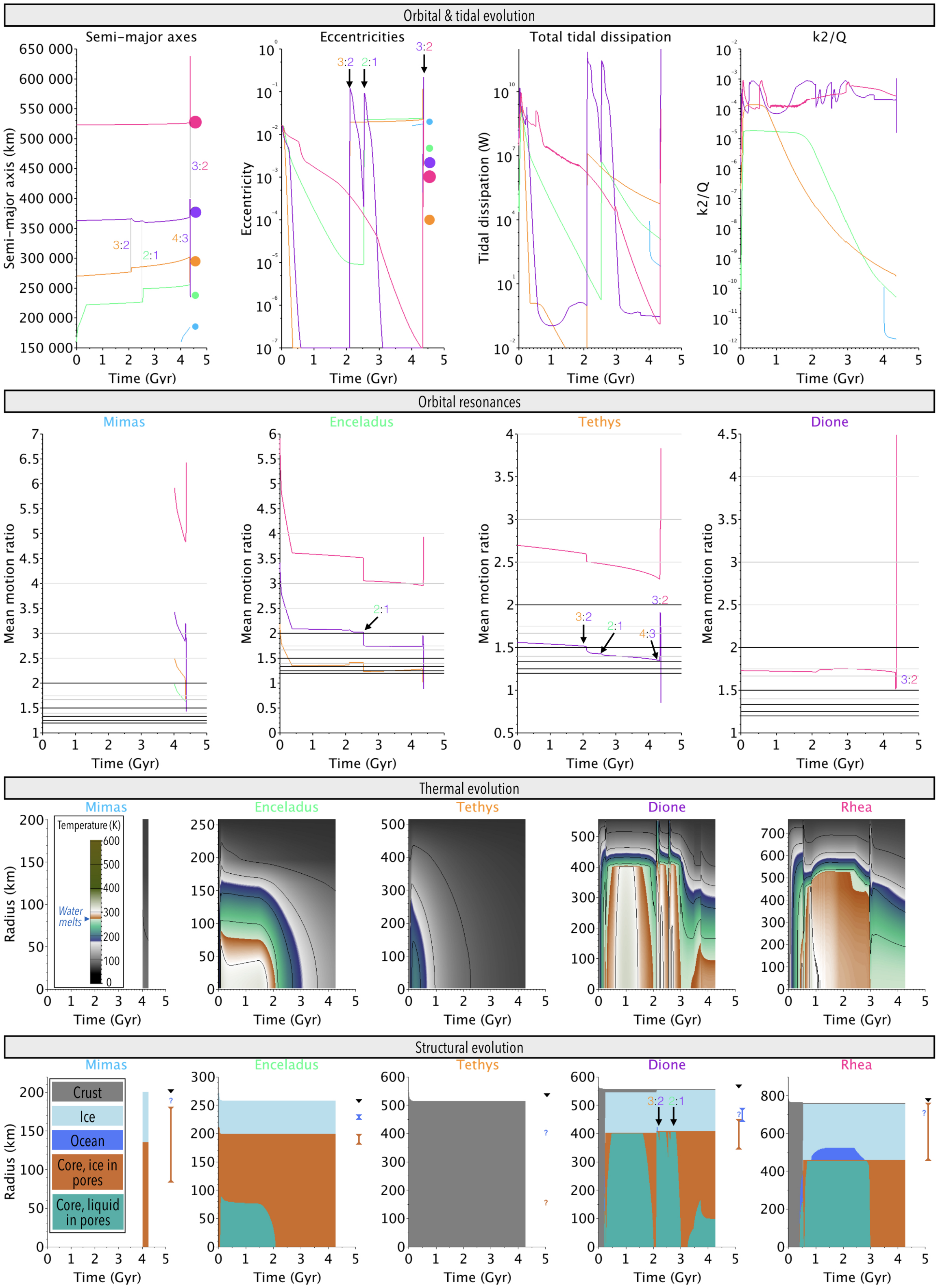

Figure 8: **Orbital, structural, and thermal evolution of Saturn's mid-sized moons for a case similar to that shown in Fig. 2 (Saturn Q=80000 initially), but with the averaged Hamiltonian model.** The legend is the same as for Supp. Fig. 7.

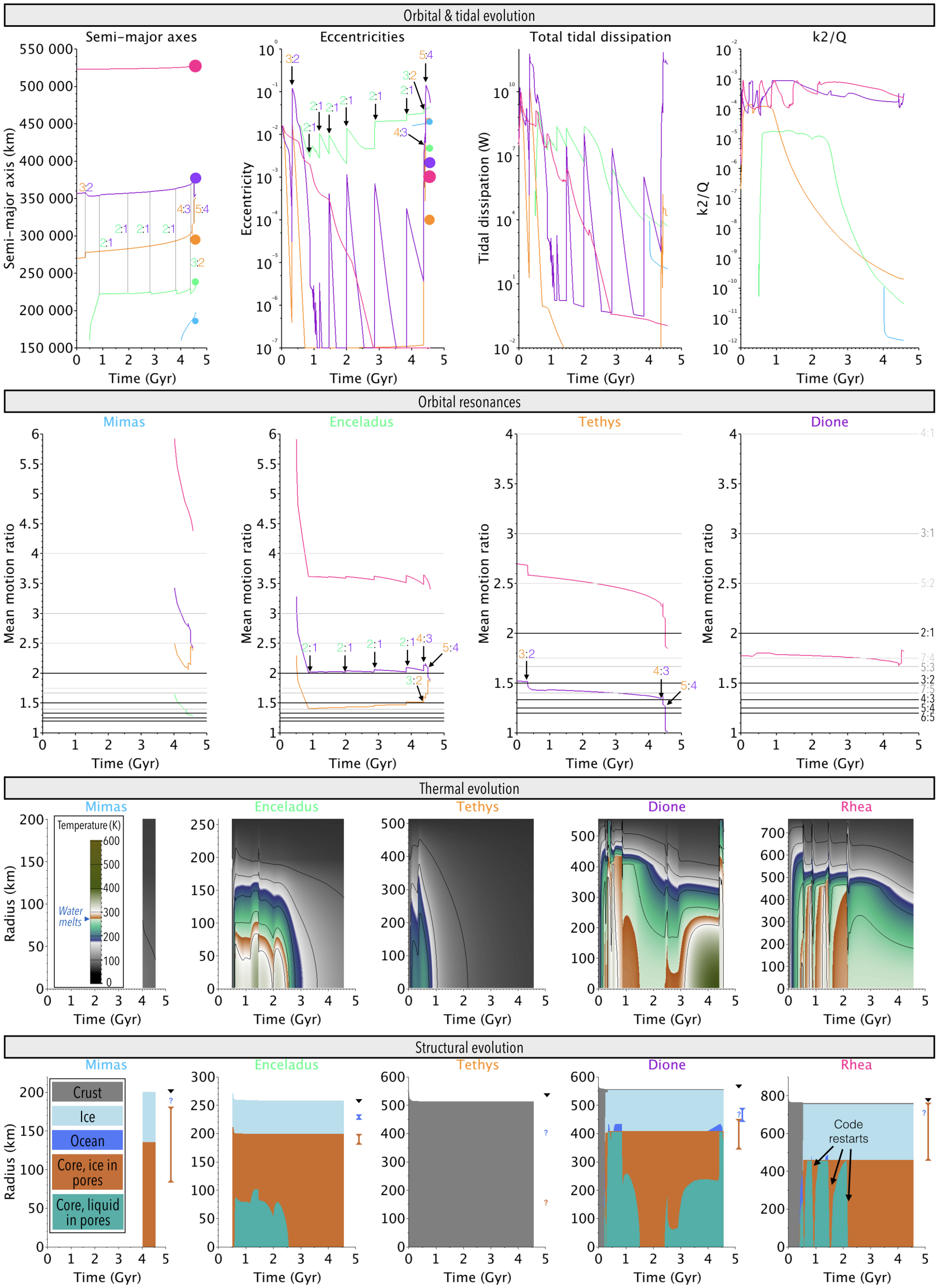

Figure 9: **Orbital, structural, and thermal evolution of Saturn's mid-sized moons for a case similar to that shown in Fig. 2 (Saturn Q=80000 initially), but with the averaged Hamiltonian model.** The legend is the same as for Supp. Fig. 7.

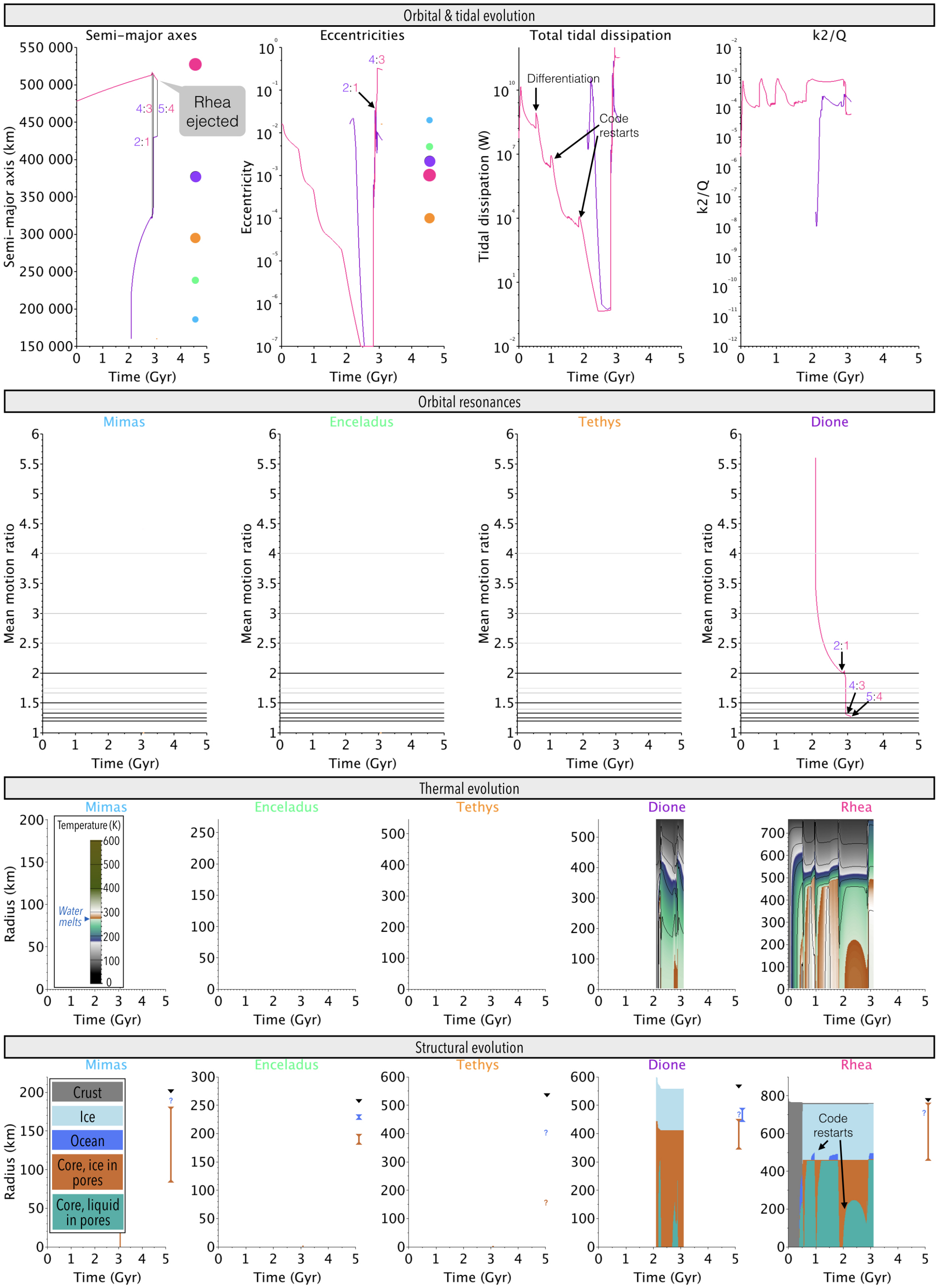

Figure 10: **Orbital, structural, and thermal evolution of Saturn's mid-sized moons for a case similar to that shown in Fig. 3 (Saturn Q=2452.8 constant), but with the averaged Hamiltonian model.** The legend is the same as for Supp. Fig. 7.

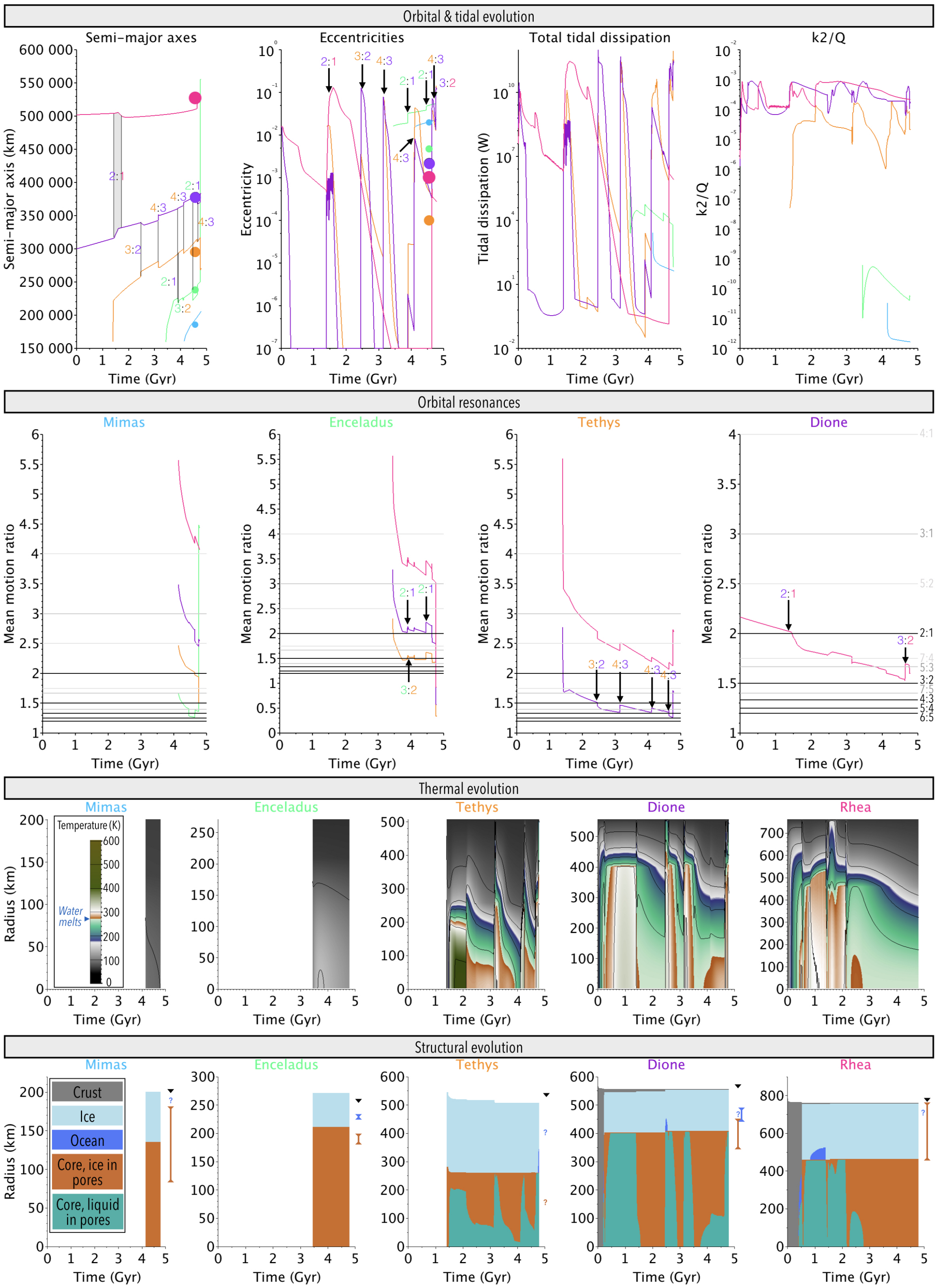

Figure 11: **Orbital, structural, and thermal evolution of Saturn's mid-sized moons for a case similar to that shown in Supplementary Fig. 3 (Saturn Q=20000 initially), but with the averaged Hamiltonian model.** The legend is the same as for Supp. Fig. 7.

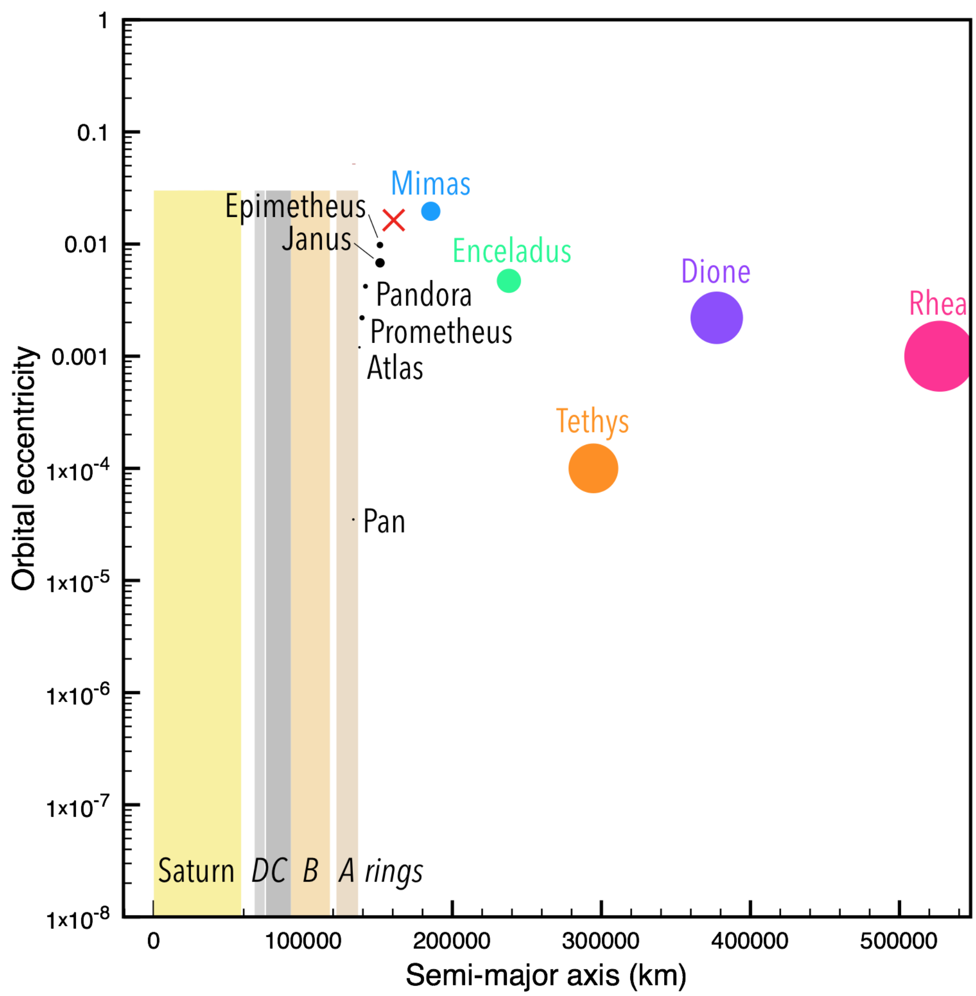

Figure 12: **Present-day orbital parameters of inner Saturn system bodies, showing an increasing trend in eccentricity with semi-major axis for small moons up to Mimas.** We assumed moons forming from the rings would follow this trend and accordingly set their starting orbital parameters in a-e space at the red "X", which is also at an eccentricity such that Mimas ends at its present-day eccentricity without excitation by interactions with other moons or damping by internal dissipation.

Supplementary Data Sets

Simulation files used to make Fig. 2 and 3 as well as all Supplementary Figures are provided as .zip archives. Each archive folder comprises, for each moon, output files describing the following quantities at 10 Myr intervals (1 Myr intervals for simulations with the averaged Hamiltonian model), from 0 to 4.5 Gyr. For each file name, the initial character `x` is `0` for the moon closest in (generally Mimas) and increases outward: `1` for Enceladus, `2` for Tethys, `3` for Dione, `4` for Rhea, and in one case `5` for Titan.

- `xCrack_depth.txt`: The cracking depth inside the rocky core over time (two columns: time in Gyr, depth of deepest cracked zone in km)

- `xCrack_stresses.txt`: Internal stresses accounted for by the core cracking subroutine (Neveu et al., 2015). There are 200 rows (one per layer from the center to the surface) printed at each time interval. Columns list, respectively: layer radius (in km), pressure in this layer (in MPa), brittle strength of this layer (in MPa), critical stress intensity in this layer (in MPa $m^{0.5}$), stress intensity from thermal expansion mismatch at grain boundaries (in MPa $m^{0.5}$), pore fluid pressure (in MPa), net pressure (stress) resulting from rock hydration (in MPa), old crack size prior to hydration/dehydration (in m), old crack size prior to mineral dissolution/precipitation (in m), current crack size (in m). Outputs are zero outside of the core.

- `xCrack_WRratio.txt`: The bulk water:rock mass ratio in the fractured zone (two columns: time in Gyr, water:rock ratio by mass in cracked zone). Outputs are zero if the core is not cracked or if there is no liquid.

- `xCrack.txt`: Lists which core layers are fractured, and by which process (Neveu et al., 2015). There are 200 columns for each layer from the center to the surface, and 451 rows for each time interval starting at 0 Gyr and ending at 4.5 Gyr. Each value is an integer: 0 = no cracks; 1 = cracks from thermal contraction; 2 = cracks from thermal expansion; 3 = cracks from hydration; 4 = cracks from dehydration; 5 = cracks from pore water dilation; 6 = mineral dissolution widening; 7 = mineral precipitation shrinking; –1 = mineral precipitation clogging; –2: clogging from hydration swelling. Outputs are zero outside of the core.

- `xHeats.txt`: Cumulative heats (in erg) produced or consumed by endogenic and exogenic processes. The six columns describe: time (in Gyr), radiogenic heat, gravitational heat, heat of rock hydration, heat consumed in rock dehydration, and heat from tidal dissipation.

- `xOrbit.txt`: Orbital parameters (three columns: time in Gyr, semi-major axis in km, eccentricity). Outputs obtained with the averaged Hamiltonian model (Supplementary §1) include 9 columns: time in Gyr, semi-major axis in km, osculating semi-major axis in km (0 if no resonance), eccentricity, product of eccentricity and cosine of resonant angle, product of eccentricity and sine of resonant angle, resonant angle in degrees, total tidal dissipation in W, and equivalent k_2/Q for the moon (Segatz et al., 1988).

- `xResonances.txt` (only for outputs obtained without the improved model of moon-moon interactions described in Supplementary §1): Moon-moon resonances encountered (time in Myr, moon undergoing the interaction and its mean motion in s^{-1}, moon causing the interaction and its mean motion in s^{-1}, nature of the resonance ($j + k : j$), rate of change in eccentricity de/dt in s^{-1}, if any).

- `xThermal.txt`: There are 200 rows for each layer, repeated 451 times, i.e. for each time interval. Columns list, respectively: layer radius (in km), layer temperature (in K); masses (in g) of rock, water ice, ammonia dihydrate (always zero here), liquid water, and liquid ammonia (always zero here) in the layer; Nusselt number in the shell (if >1, the shell convects); fraction of amorphous ice in the layer (always zero here); thermal conductivity of the layer (in W m^{-1} K^{-1}); degree of hydration of the layer (0: fully dry; 1: fully hydrated); and porosity of the layer.

- `xTidal.txt`: Rates of tidal heating in each layer in W (200 rows for each layer, repeated 451 times, i.e. for each time interval).

In addition, each folder contains the following files:

- `IcyDwarfInputs.txt`: Simulation input file.

- `Primary.txt`: Over time in Gyr (first column), the Q of Saturn (second column) and the mass of its ring in kg (third column).

Outputs obtained with the averaged Hamiltonian model include the following files. Each output is read in $N_{\text{moon}} \times N_{\text{moon}}$ matrices, where N_{moon} is the number of moons. Matrices are typically 5×5. Matrices are symmetric since they describe interactions between pairs of moons. Element (x, y) represents interactions between the x^{th} and y^{th} innermost moons. From innermost to outermost, the moons are Mimas, Enceladus, Tethys, Dione, and Rhea (e.g. third row – first column: Mimas-Tethys). The first matrix is output at the first time step. Subsequent matrices are output following a time stamp that corresponds to the time at which pairs of moons get in and out of resonance.

- `Resonances.txt`: Values are integers j if the mean motions of the corresponding moons are commensurate in $j + 1 : j$ ratios with $j \leq 5$, and if the migration of the moons is convergent ($j\ dn_{\text{inner moon}}/dt \leq (j + 1)\ dn_{\text{outer moon}}/dt$ since $dn/dt < 0$ for expanding orbits). Values are 0 otherwise. If a moon is in resonance with only one other moon, the code computes moon-moon interactions (value in `ResAcctFor` below $= j$), otherwise interactions may be ignored (value in `ResAcctFor` $= 0$).

- `ResAcctFor.txt`: Stands for "Resonances Accounted For". A nonzero value in `Resonance` above is accounted for if a moon is in resonance with only one other moon. Otherwise, the code cannot compute the orbital evolution resulting from the interactions between more than two moons. In that case, the resonance accounted for is that between the pair of moons for which j is smallest (resonance for which the most moon-moon conjunctions occur per orbit). For equal values of j (e.g. for a 4:2:1 resonance, j would be 1 between the inner and middle moon, and also 1 between the middle and outer moon), the newer resonance is ignored. For moons with nonzero values, orbital evolution is computed by the full routine described in Supp. §1. Otherwise, orbital evolution is computed solely due to effects from moon-primary and moon-ring interactions, ignoring moon-moon interactions.
- `PCapture.txt`: This output is not taken into account in computations, but provides an indicative probability of capture into resonance based on the equations of Borderies and Goldreich (1984). Whether or not capture occurs in a simulation depends on the outcome of orbital evolution computed with the averaged Hamiltonian routine (Supplementary §1). This matrix is not made symmetric, so usually the value of a coefficient in a position symmetric to that of a nonzero value is 0. In that case, only the nonzero value is meaningful.

References

Asphaug, E. and Reufer, A. Late origin of the Saturn system. *Icarus*, 223(1):544–565, 2013. URL `http://dx.doi.org/10.1016/j.icarus.2012.12.009`.

Baland, R.-M., Tobie, G., Lefèvre, A., and Van Hoolst, T. Titan's internal structure inferred from its gravity field, shape, and rotation state. *Icarus*, 237:29–41, 2014. URL `https://doi.org/10.1016/j.icarus.2014.04.007`.

Borderies, N. and Goldreich, P. A simple derivation of capture probabilities for the $j+1$:j and $j+2$:j orbit-orbit resonance problems. *Celestial Mechanics*, 32(2):127–136, 1984. URL `https://doi.org/10.1007/BF01231120`.

Ćuk, M., Dones, L., and Nesvornỳ, D. Dynamical evidence for a late formation of Saturn's moons. *The Astrophysical Journal*, 820(2):97, 2016. URL `http://dx.doi.org/10.3847/0004-637X/820/2/97`.

Jacobson, R. A., Antreasian, P. G., Bordi, J. J., Criddle, K. E., Ionasescu, R., Jones, J. B., Mackenzie, R. A., Meek, M. C., Parcher, D., Pelletier, F. J., Owen, W. M., Roth, D. C., Roundhill, I. M., and Stauch, J. R. The gravity field of the saturnian system from satellite observations and spacecraft tracking data. *The Astronomical Journal*, 132(6): 2520, 2006. URL `https://doi.org/10.1086/508812`.

Malhotra, R. Orbital resonances and chaos in the solar system. In *Solar System Formation and Evolution*, volume 149, page 37, 1998.

Meyer, J. and Wisdom, J. Tidal evolution of Mimas, Enceladus, and Dione. *Icarus*, 193: 213–223, 2008. URL `https://doi.org/10.1016/j.icarus.2007.09.008`.

Murray, C. D. and Dermott, S. F. *Solar System Dynamics*. Cambridge University Press, 1999.

Neveu, M., Desch, S. J., and Castillo-Rogez, J. C. Core cracking and hydrothermal circulation can profoundly affect Ceres' geophysical evolution. *Journal of Geophysical Research: Planets*, 120:123–154, 2015. URL `http://dx.doi.org/10.1002/2014JE004714`.

Press, W. H., Teukolsky, S. A., Vetterling, W. T., and Flannery, B. P. Integration of ordinary differential equations. In *Numerical Recipes in C*, pages 707–752. Cambridge University Press, 2002.

Salmon, J. and Canup, R. M. Accretion of Saturn's inner mid-sized moons from a massive primordial ice ring. *The Astrophysical Journal*, 836(1):109, 2017. URL `https://doi.org/10.3847/1538-4357/836/1/109`.

Segatz, M., Spohn, T., Ross, M. N., and Schubert, G. Tidal dissipation, surface heat flow, and figure of viscoelastic models of Io. *Icarus*, 75(2):187–206, 1988. URL `https://doi.org/10.1016/0019-1035(88)90001-2`.

Sohl, F., Solomonidou, A., Wagner, F. W., Coustenis, A., Hussmann, H., and Schulze-Makuch, D. Structural and tidal models of Titan and inferences on cryovolcanism. *Journal of Geophysical Research: Planets*, 119(5):1013–1036, 2014. URL `https://doi.org/10.1002/2013JE004512`.

Zhang, K. and Nimmo, F. Recent orbital evolution and the internal structures of Enceladus and Dione. *Icarus*, 204:597–609, 2009. URL `https://doi.org/10.1016/j.icarus.2009.07.007`.